Prepared for submission to JHEP DAMTP-2017-03-06

arXiv:1703.00914v2 [hep-ph] 24 Apr 2017

Fractal based observables to probe jet substructure of quarks and gluons

Joe Davighi,[a] **Philip Harris**[b]

[a] *Department of Applied Mathematics and Theoretical Physics, University of Cambridge, Wilberforce Road, Cambridge, UK*

[b] *CERN, European Organization for Nuclear Research, Geneva, Switzerland*

E-mail: jed60@cam.ac.uk, philip.coleman.harris@cern.ch

Abstract: New jet observables are defined which characterize both fractal and scale-dependent contributions to the distribution of hadrons in a jet. These infrared safe observables, named Extended Fractal Observables (EFOs), have been applied to quark-gluon discrimination to demonstrate their potential utility. The EFOs are found to be individually discriminating and only weakly correlated to variables used in existing discriminators. Consequently, their inclusion improves discriminator performance, as here demonstrated with particle level simulation from the parton shower.

Contents

1 Introduction **1**

2 Extended Fractal Observables **2**
2.1 Variable definitions 2
2.2 The range of box-counting scales 5
2.3 Infrared and Collinear safety 6

3 Performance in Quark-Gluon Discrimination **7**
3.1 Results 7

4 Conclusions **9**

5 Outlook **9**

6 Acknowledgments **10**

1 Introduction

A hadronic jet is produced from an initial parton via a sequence of perturbative QCD branching interactions (the parton shower), followed by the non-perturbative conversion of partons to the hadrons we observe in experiments (hadronization). A Markov chain description of the parton shower suggests the spatial distribution of partons will exhibit some fractal character [1–6], and this will be inherited by the final hadron distribution (invoking local parton-hadron duality [7]). However, true scale invariance of the hadron distribution within a jet is broken by the running of the branching probability, termination of the shower due to hadronization, and finite detector resolution. Here we define new observables to characterize jet branching structure, named Extended Fractal Observables (EFOs), which accommodate deviations from fractal structure through simple parametrizations. The idea is to apply box-counting techniques, used widely in the study of dynamical systems and scale invariant objects, to the substructure of QCD jets. Box counting has previously been employed in particle physics to calculate the fractal dimension of electromagnetic showers [8] for highly granular calorimetric reconstruction. Here, we extend the generality and information content of this technique in our characterization of QCD jets.

The motivation for this study is two-fold. Firstly, we would like to characterize the spatial substructure of jets into a set of new observables. Secondly, we would like to demonstrate the use of such observables in the discrimination of quark and gluon jets. Quark and gluon

discrimination has long been used as a tool to enhance the sensitivity of signatures with additional quarks [9, 10]. In particular weak boson fusion induced Higgs-production is enhanced due to the distinct signature of two additional hard quark jets in the gluon-dominated forward region of the detector [9, 11–19]. Quark and gluon tagging are also expected to be useful for physics searches *beyond* the Standard Model, including the detection of supersymmetric particles [20, 21]. Additionally, if well designed, these taggers can be further extended to the subjets of boosted boson signatures [22]. We demonstrate that modest improvements can be made to existing quark-gluon taggers by incorporating the new jet observables defined in this paper.

Finally, our construction of pixel-based jet observables resonates with the recent development of the jet image paradigm [23, 24], in which the energy measured in each detector cell is interpreted as the intensity of a pixel in a 2D image. Within this approach, powerful machine-learning algorithms for classifying images have been brought to bear on a range of jet classification problems. This has included tagging boosted weak bosons [24, 25], boosted top quarks [26], and heavy-flavors [27, 28].

We define EFOs in the following section. In section 3 we analyze the performance of these observables in quark-gluon discrimination, before concluding.

2 Extended Fractal Observables

The computation of the EFOs is performed on a jet by jet basis using a variation of the Minkowski-Bouligand (box-counting) dimension. For the purpose of these studies, QCD dijet samples are produced and showered at leading order using Herwig++ [29] at a center-of-mass energy of 8 TeV. Jets are clustered with the anti-kt algorithm using the final state particles following showering and hadronization; a cone size of $R = 0.4$ and the fastjet code package [30] are used for the jet clustering. The EFOs are computed for the leading jet in each event (a typical jet energy being 100 GeV), subject to a minimum jet p_T of 50 GeV. The choice of Herwig for quark gluon discrimination provides for a conservative estimate of the discrimination power [31] when compared with either Large Hadron Collider (LHC) data or other parton shower algorithms.

2.1 Variable definitions

To define our variables we implement a two-stage recipe: firstly, the jet cone is divided in the familiar (η, ϕ) angular coordinates into a square grid of cells, each cell having side-length ϵ. For a given scale ϵ, we count the number of cells $N_{hits}(\epsilon)$ which register particle hits with a total transverse momentum greater than some pixel-level soft cutoff, in this study chosen to be $p_T > 0.1$ GeV. This low energy cut represents a limiting threshold due to detector resolution. This counting is iterated over a range of scales, as is illustrated in Figure 1. The second stage is to fit smooth functions to the variation of $y = \log N_{hits}(\epsilon)$ with $x = \log(1/\epsilon)$, and to extract the parameters of the fit as a set of (correlated) jet observables, which we

call Extended Fractal Observables (EFOs). This is a generalization of the traditional box-counting method, in which only linear functions $y = mx + c$ are fitted, with the gradient m identified as the fractal dimension [8].

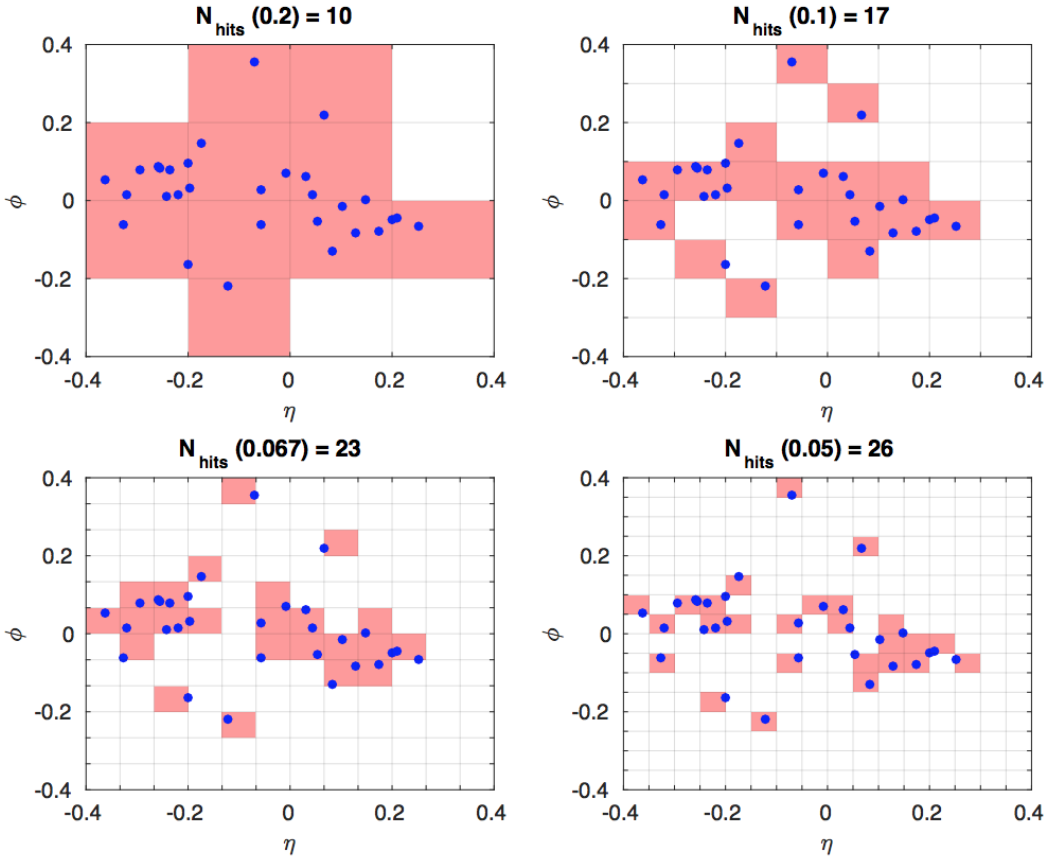

Figure 1. An illustration of the iterated box-counting procedure used to calculate fractal-based quantities on a set of points. The filled blue circles are the (η, ϕ) angular coordinates of the hadrons within a particular sample jet (in particular, this jet has total $p_T = 157$ GeV, and 30 constituent hadrons). The box-counting is illustrated for four sample scales, corresponding to successively finer ϵ values of 0.2, 0.1, 0.067 and 0.05. The cells registering particle hits are highlighted with red shading.

Indeed, in Figure 2 we do not observe any distinct region of linear scaling, as would be needed to extract a fractal dimension. Rather, $\log N_{hits}(\epsilon)$ levels off smoothly from large to small scales, ultimately saturating as a result of hadronization. This continuous scale dependence motivates our use of non-linear fitting functions, which significantly extend the information content available. In particular, the hadronization region carries residual information from quark-gluon discrimination, which we aim to extract through these newly defined

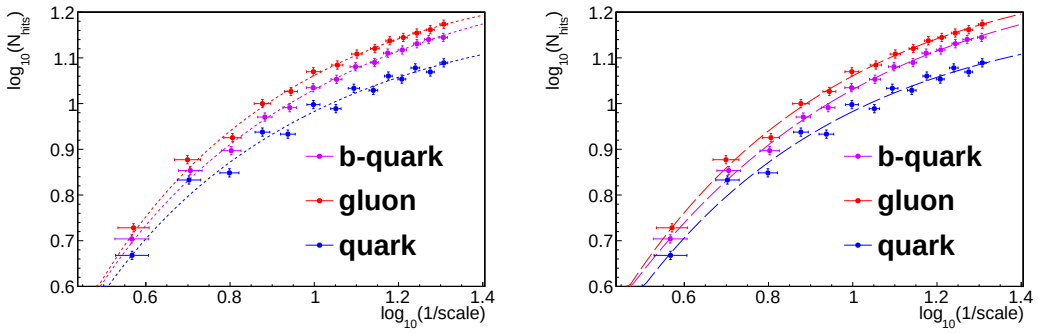

Figure 2. Left: logarithmic fits to $\log N_{hits}(\epsilon)$ against $\log(1/\epsilon)$ for light quarks, bottom quarks, and gluons, of the form $y = p_0 + p_1 x + p_2 \log x$. The values of the fitted parameters $\{p_i\}$ define one possible set of Extended Fractal Observables. Right: fits to $\log(N_{hits})$ against $\log(1/\epsilon)$ using an asymptotically saturating fitting function, specifically $y = p_0 + p_1 \tanh(x - p_2)$.

observables. We considered three different three-parameter fitting functions to demonstrate the method:

1. logarithmic fits of the form $y = p_0 + p_1 x + p_2 \log x$ (see Figure 2).
2. quadratic fits: $y = p_0 + p_1 x + p_2 x^2$.
3. hyperbolic tangent fits: $y = p_0 + p_1 \tanh(x - p_2)$.

The first two fitting functions are designed to capture the variation of box-counting with scale in the parton-shower region, rather than its asymptotic saturation in the hadronization region (note that they do not saturate). Moreover, the simplicity of these functions allows greater freedom when fitting to data, where not everything is well-modeled. If desired, one could rather fit functions which saturate to more faithfully capture the hadronization region, for example the hyperbolic tangent parametrization we have fitted in Figure 2; however, it's not clear this would give additional discrimination power, because this asymptotic information is strongly correlated with the jet multiplicity.

The values of the best fit parameters $\{p_i\}$ for each fitting function constitute three possible sets of EFOs. While all three fits were capable of modeling the distribution, in the following section we shall focus on the so-called logarithmic fits because of their greater discrimination power between quarks and gluons. These logarithmic fits are displayed for jets in Figure 2, along with the fits to the asymptotically saturating parametrization. The observed scaling is distinct between quarks, gluons and b-quarks (see Figure 3). This scaling is a fundamental property of QCD resulting from the splitting of quarks and gluons. Further measurements of this scaling allows for an alternative approach to extract QCD properties such as the strong coupling constant [32, 33].

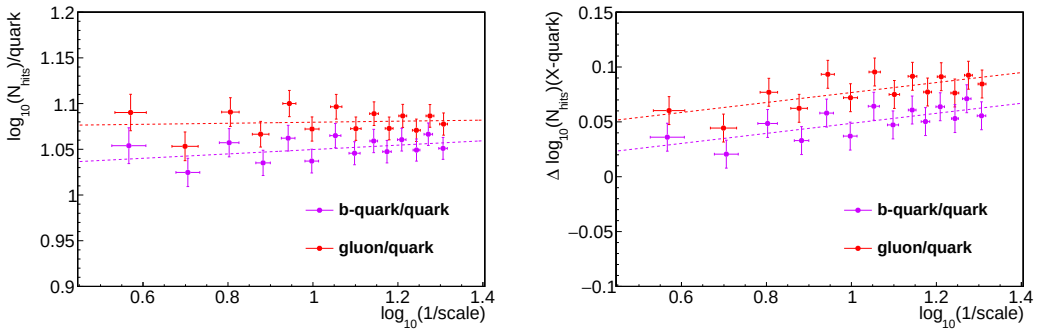

Figure 3. Left: the *ratio* of $\log(N_{hits})$ with respect to the quark values, for b-quarks and gluons, as a function of $\log(1/\epsilon)$. A linear fit is added for comparison. Right: the *difference* of $\log(N_{hits})$ with respect to the quark values, for b-quarks and gluons. In the Modified Leading Logarithmic Approximation (MLLA), the differences in hadron multiplicity between quarks, b-quarks and gluons are predicted to be energy independent [34]. The small but non-zero slopes in this plot reflect the fact that box-counting at a given angular scale probes spatial information in addition to the rate of splitting at the corresponding energy scale.

2.2 The range of box-counting scales

The range of angular scales ϵ has been chosen by paving the jet cone with a square grid of $N \times N$ cells, where the splitting scale N ranges in integer steps from 3 to 16. For each N, the angular scale is $\epsilon = 2R/N$, where R is the jet radius. The coarsest ϵ scale chosen, corresponding to $N = 3$, is essentially the coarsest scale carrying potentially discriminating information (for $N = 2$ the jet cone would be divided into four quarters, all of which will register a hit for realistic jet shapes). The finest ϵ scale chosen is $\epsilon_{min} = 0.8/16 = 0.05$. This is a suitable cut-off scale for two reasons. Firstly, this is approximately the angular detector resolution in both LHC experiments, CMS and ATLAS [35, 36]. Secondly, for the 100 GeV jets studied here, the number of hits is saturating at this scale (see Figure 2), and so any further subdivision of the jet cone would yield negligible additional information.

The appropriate saturation scale varies with the jet energy, and can be estimated using the jet multiplicity. At 100 GeV, a toy computation for a typical hadron multiplicity of 30 yields $< 2\%$ expected overlap in the particle content per cell when $N = 16$. This sets the finest splitting scale N_{split} needed at our reference energy. To extrapolate to an average jet energy Q^2, we can exploit the leading order scaling of the jet multiplicity, $M(Q^2)$ [15]:

$$M(Q^2) \sim M_0 + K\alpha_s(Q^2)^{\frac{1}{4}+\frac{2n_f}{3\beta_0}\left(1-\frac{C_A}{C_F}\right)} \exp\left(\sqrt{\frac{32C_A\pi}{\beta_0^2\alpha(Q^2)}}\right), \tag{2.1}$$

where M_0 and K are non-perturbative constants, $\alpha_S(Q^2)$ the strong coupling, n_f the number of active quark flavors, β_0 the one-loop QCD beta function, and C_A, C_F are the QCD color

factors. The second term on the right hand side, which gives the scaling with Q^2, is the leading order perturbative contribution [37]. Higher order formulae for the particle multiplicity have been calculated in recent years [38, 39], which depend on only one empirical normalization constant. However, for our purpose of suggesting the finest splitting scale to use in the EFO computation, the leading order expression given above is sufficient. Then, given this multiplicity scaling, the scaling of the required finest splitting scale with jet energy is, to lowest order in the small quantity $\mu = \frac{M}{N_{split}^2}$ (i.e. the mean number of particles per smallest-scale box):

$$N_{split}(Q^2) = N_{split}(100\text{ GeV})\sqrt{\frac{M(Q^2)}{M(100\text{ GeV})}}, \tag{2.2}$$

where our reference is $N_{split}(100\text{ GeV}) = 16$. For example, this scaling suggests one should use a finest splitting scale of $N_{split}(1\text{ TeV}) = 20$ for 1 TeV jets.

Finally, we would like to highlight that these fractal-based observables are similar in spirit to calculating subjet rates of jets [13, 40], given subjets clustered using the p_T-independent Cambridge-Aachen algorithm. Both sets of variables compute p_T-independent branching information on a succession of angular scales down to some threshold. However, the EFOs defined here do not require any further clustering algorithms to be run on the jet substructure (taking as inputs only the angular coordinates of the constituent hadrons), thereby exploiting the scaling information down to the level of hadronization.

2.3 Infrared and Collinear safety

Preserving infrared and collinear safety ensure calculability in perturbative QCD. An observable is infrared (collinear) safe if its value is unchanged by the emission of soft (co-moving) particles. The EFOs, as defined in 2.1 with a pixel-level soft cutoff, are fully IRC safe.

Firstly, the box counting procedure is intrinsically collinear safe: if one particle splits into two particles with the same (η, ϕ) coordinates, we still count just one cell hit by both daughter particles, at any finite scale of probing. Hence collinear splittings will not affect the number of cells $N_{hits}(\epsilon)$ to register particle hits at any choice of scale. On the other hand, infrared safety of the EFOs can only be engineered by imposing some low momentum cutoff to cleanse the jet of its soft constituents. However, this soft cutoff must be implemented consistently with collinear safety. If we simply discarded all soft hadrons with, say $p_T < 0.1$ GeV, this would spoil collinear safety. To see this, consider the following pathological example: if a particle with $p_T = 0.15$ GeV splits into two comoving particles with $p_T = 0.08$ GeV and $p_T = 0.07$ GeV, then both would be discarded by a particle-level soft cut, and so $N_{hits}(\epsilon)$ would not be invariant under this collinear splitting.

This is remedied by defining a pixel-level (rather than particle-level) sort cutoff. That is, we only consider a cell to register a hit if it measures a total p_T greater than our soft cutoff of 0.1 GeV. This way, if the troublesome 0.15 GeVparticle in the example above splits collinearly into any number of daughters, the pixel still measures a total p_T of 0.15 GeV, and so registers a hit regardless of these splittings. Thus, box-counting with a pixel-level soft cutoff is fully

IRC safe. In addition, a pixel-level rather than particle-level cut is more naturally realized experimentally since a pixel hit is consistent with an LHC detectors cell. Pixel-level cutoffs have been used previously in the context of jet images analyses (for example in [23]) to ensure IRC safety in the same context.

3 Performance in Quark-Gluon Discrimination

To assess the level of quark and gluon discrimination (QGD) power, we define the flavor of a jet by searching through the generated partonic history and matching each jet to the highest-p_T parton within $R < 0.3$ of the jet axis. The flavor of the jet is then identified with that of the matched parton. All jet observables have been calculated for the highest p_T jet in each event. An event is classified as signal (background) if the leading jet is matched to a quark (gluon)[1].

As a baseline for comparison, we consider the variables currently used by the Compact Muon Solenoid (CMS) quark-gluon tagger, which are [10]: i) the number of particles in the jet (multiplicity) [41]; ii) the $p_T D$ variable ($C_1^{\beta=0}$)[42], which describes the distribution of transverse momentum between the particles in the jet, defined as $p_T D = \frac{\sqrt{\Sigma_i p_{T,i}^2}}{\Sigma_i p_{T,i}}$; iii) the semi-minor axis of the jet in the $\eta - \phi$ plane, denoted σ_2. The EFOs are found to add more discriminatory power when using the logarithmic fitting function, and so we focus on this choice of non-linear parametrization here.

3.1 Results

Figure 4 presents the linear correlation coefficients between the EFOs and the three variables currently used in the CMS quark-gluon tagger: multiplicity, $p_T D$ and σ_2. Strong correlations are present amongst the EFOs, as is natural given they are parameters derived from the same fit. However, their correlations with the additional jet parameters are no greater than 42%. Interestingly, the EFOs are most highly correlated with the σ_2 variable, not jet multiplicity as might have been expected.

We compare the quark-gluon discrimination power of individual jet variables by plotting receiver operating characteristics (ROCs) in Figure 5. While the combination of all three EFOs adds little discrimination beyond that of a single EFO due to their near-perfect correlation, the selection of any single p_i would be arbitrary for the sake of this comparison. We have therefore used their combination to construct a Boosted Decision Tree (BDT) discriminator for use in this comparison. Figure 5 shows that the EFOs are individually well-discriminating, particularly if we seek high signal efficiency. Their performance is significantly better than that of the jet multiplicity variable: this, together with the evidence from the correlation matrices, suggests the discrimination power of the EFOs is not simply a result

[1] Note that this signal definition includes b-jets (jets initiated by bottom quarks), which may be efficiently identified using a secondary vertex tagger, and separately vetoed. Since the properties of b-jets are typically closer to those of gluon jets, quark-gluon discrimination will be further improved by vetoing b-jets.

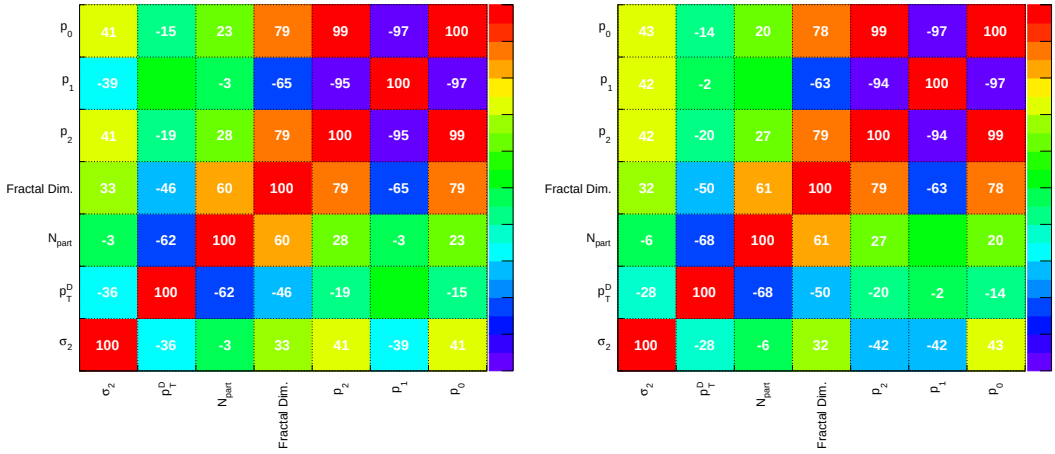

Figure 4. Correlation matrices, displaying the linear correlation coefficients between pairs of variables. We include the existing QGD variables (multiplicity, $p_T D$ and σ_2), the EFOs introduced in this paper, and also the Minkowski-Bouligand dimension (labeled Fractal Dim.), which has been calculated from a linear fit over a small range of box scales. The left matrix is for quark jets (signal) and the right for gluon jets (background). The three individual EFO parameters, p_0, p_1 and p_2, are almost perfectly correlated to each other as would be expected. Importantly, we see only weak correlations between the EFOs and the three existing QGD variables. Note that the traditional fractal dimension is much more strongly correlated to existing QGD variables, particularly multiplicity.

of higher multiplicities in gluon and bottom jets. These results indicate that the addition of these parameters to a quark-gluon discriminator can improve performance.

The right plot of Figure 5 validates this claim, by plotting the gain in discrimination achieved by replacing multiplicity with the EFOs. This gain, though modest, is greater than the gain given by including multiplicity in the existing discriminator in the first place. For a quark efficiency of 60%, we have respective gluon rejection rates of 67.5% for a BDT discriminator constructed using only $p_T D$ and σ_2, 68.4% using $p_T D$, σ_2 and multiplicity (the existing discriminator), and 69.6% using $p_T D$, σ_2 and the EFOs (our new discriminator). Note that combining all four variables was seen to give negligible further improvement. This suggests all the information from multiplicity is captured by the EFOs[2], while the converse is not true.

Consequently, the Extended Fractal Observables provide an additional handle that captures the most salient features of the jet multiplicity, incorporates new information from showering and hadronization, and which is also better behaved under IRC emission (see 2.3).

[2]this is unsurprising, because jet multiplicity is simply the asymptotic number of hits as we approach the saturation region.

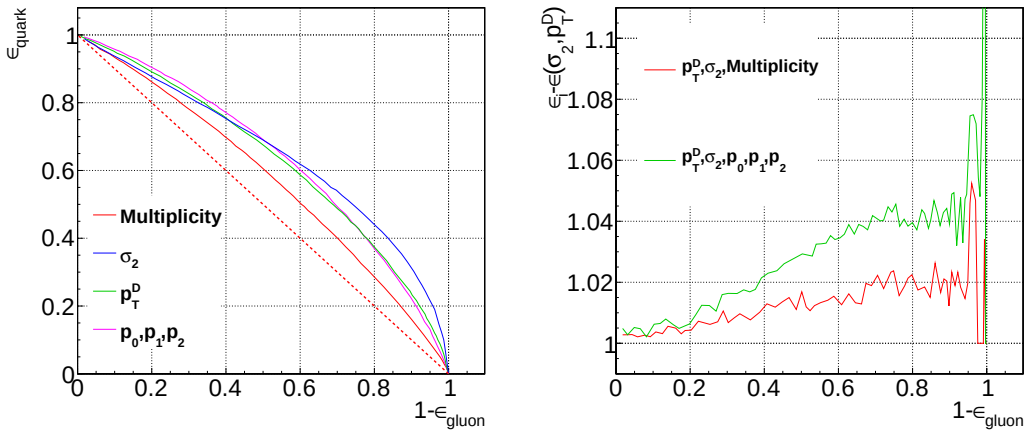

Figure 5. Left: single variable performance comparison, in terms of quark efficiency (fraction of quark jets passed by a certain cut on the discriminator variable) and gluon rejection (fraction of gluon jets rejected by that same cut). The EFOs, minor axis, and $p_T D$ are significantly more discriminating than multiplicity. The EFOs are most discriminating for high signal efficiency ($\gtrsim 70\%$), below which jet minor axis becomes most discriminating. Right: Comparison of the relative gain in signal discrimination when adding the EFOs compared with adding the particle multiplicity.

4 Conclusions

In this study we defined new jet observables, the Extended Fractal Observables, by a generalization of the box-counting method used in the study of fractal systems. Such methods are appealing by virtue of their simplicity, both conceptually and in their implementation. Defined with a pixel-level low momentum cutoff, these observables are infrared and collinear safe. We have then sought to apply the EFOs to improve quark-gluon discrimination. At the generator level, we find some modest improvement in discrimination by gluon rejection when we replace multiplicity with the EFOs in the existing tagger. Extending the performance of these new variables to include detector effects can naturally be performed in the LHC environment with the CMS Particle Flow algorithm [43] in conjunction with the PUPPI algorithm [44] to reconstruct particle candidates in the presence of high pile-up.

5 Outlook

This method of studying jet substructure is a new approach. As such, there are many directions in which we would like to proceed, including:

1. Investigating the p_T-dependence of the EFOs. The multiplicity has a logarithmic scaling with the jet p_T, and consequently we would expect the last splitting scale to have some

dependence on jet p_T. A minimum p_T cut imposed (50 GeV in this study) can further modify the shape of the EFOs.

2. Exploring particle hits in a 3-dimensional coordinate space spanned by η, ϕ and z^{-1}, where z is the fractional transverse momentum of the jet constituent.

3. Applying the EFOs beyond Quark-Gluon discrimination, for example to the identification of pile-up jets.

4. These box-counting methods extend very naturally from the substructure of a single jet to a whole-event analysis. Such a novel approach may provide new insight into searches for new physics topologies such as those in supersymmetry or top quark pair production [45].

5. Furthermore, box-counting analyses could provide a useful characterization of event shapes in heavy ion collisions, where studies of jet properties beyond jet reconstruction are traditionally difficult, but well motivated [46–48].

6. Finally, we would like to emphasize that the calculation of EFOs on quark and gluon jets probes parton shower scaling that results from the QCD color factor ratio. Calculating EFOs on cosmic ray air shower profiles [49] could therefore help discriminate QCD-induced air showers from more interesting signals; of particular interest, showers induced by electroweak sphalerons. Experimentally, the calculation of EFOs in this air shower context is conceptually appealing: the 1660 individual Cerenkov detectors (spread over 3000 km^2) of the Pierre Auger Observatory in Argentina [50] would naturally function as the finest-scale cells in our box-counting algorithm. These techniques could therefore be useful in probing physics at energies far beyond that of the LHC.

6 Acknowledgments

JD's work has been supported by The Cambridge Trust, and by the STFC consolidated grant ST/L000385/1. We thank the CERN summer student program where this work was initiated. We also thank Andrew Larkoski for his insightful comments when performing these studies, and Bryan Webber for helpful discussions. Finally, we thank Eric Metodiev for helpful comments.

References

[1] G. Gustafson and A. Nilsson, *Multifractal dimensions in QCD cascades*, *Z. Phys.* **C52** (1991) 533–542.

[2] J. D. Bjorken, *Fractal phase space as a diagnostic tool for high-energy multijet processes*, *Phys. Rev. D* **45** (Jun, 1992) 4077–4087.

[3] B. Andersson, P. Dahlkvist, and G. Gustafson, *An Infrared Stable Multiplicity Measure on QCD Parton States*, *Phys. Lett.* **B214** (1988) 604–608.

[4] A. J. Larkoski, *QCD Analysis of the Scale-Invariance of Jets*, *Phys. Rev.* **D86** (2012) 054004, [1207.1437].

[5] M. Jankowiak and A. J. Larkoski, *Angular Scaling in Jets*, *JHEP* **04** (2012) 039, [1201.2688].

[6] D. E. Soper and M. Spannowsky, *Finding physics signals with shower deconstruction*, *Phys. Rev.* **D84** (2011) 074002, [1102.3480].

[7] Y. L. Dokshitzer, V. A. Khoze, and S. I. Troyan, *On the concept of local parton-hadron duality*, *Journal of Physics G: Nuclear and Particle Physics* **17** (1991), no. 10 1585.

[8] M. Ruan, D. Jeans, V. Boudry, J.-C. Brient, and H. Videau, *Fractal Dimension of Particle Showers Measured in a Highly Granular Calorimeter*, *Phys. Rev. Lett.* **112** (2014), no. 1 012001, [1312.7662].

[9] **ATLAS** Collaboration, G. Aad et al., *Light-quark and gluon jet discrimination in pp collisions at $\sqrt{s} = 7$ TeV with the ATLAS detector*, *Eur. Phys. J.* **C74** (2014), no. 8 3023, [1405.6583].

[10] **CMS Collaboration** Collaboration, *Performance of quark/gluon discrimination in 8 TeV pp data*, Tech. Rep. CMS-PAS-JME-13-002, CERN, Geneva, 2013.

[11] D. Ferreira de Lima, P. Petrov, D. Soper, and M. Spannowsky, *Quark-Gluon tagging with Shower Deconstruction: Unearthing dark matter and Higgs couplings*, *Phys. Rev.* **D95** (2017), no. 3 034001, [1607.06031].

[12] J. Gallicchio and M. D. Schwartz, *Quark and Gluon Jet Substructure*, *JHEP* **04** (2013) 090, [1211.7038].

[13] J. Gallicchio and M. D. Schwartz, *Quark and Gluon Tagging at the LHC*, *Phys. Rev. Lett.* **107** (2011) 172001, [1106.3076].

[14] J. Gallicchio and M. D. Schwartz, *Pure Samples of Quark and Gluon Jets at the LHC*, *JHEP* **10** (2011) 103, [1104.1175].

[15] **DELPHI** Collaboration, P. Abreu et al., *The Scale dependence of the hadron multiplicity in quark and gluon jets and a precise determination of C(A) / C(F)*, *Phys. Lett.* **B449** (1999) 383–400, [hep-ex/9903073].

[16] **CLEO** Collaboration, R. A. Briere et al., *Comparison of particle production in quark and gluon fragmentation at s**(1/2) 10-GeV*, *Phys. Rev.* **D76** (2007) 012005, [0704.2766].

[17] J. Pumplin, *Quark - gluon jet differences at LEP*, *Phys. Rev.* **D48** (1993) 1112–1116, [hep-ph/9301215].

[18] M. H. Seymour, *The Subjet multiplicity in quark and gluon jets*, *Phys. Lett.* **B378** (1996) 279–286, [hep-ph/9603281].

[19] C. Kilic, S. Schumann, and M. Son, *Searching for Multijet Resonances at the LHC*, *JHEP* **04** (2009) 128, [0810.5542].

[20] B. Bhattacherjee, S. Mukhopadhyay, M. M. Nojiri, Y. Sakaki, and B. R. Webber, *Quark-gluon discrimination in the search for gluino pair production at the LHC*, *JHEP* **01** (2017) 044, [1609.08781].

[21] K. Joshi, A. D. Pilkington, and M. Spannowsky, *The dependency of boosted tagging algorithms on the event colour structure*, *Phys. Rev.* **D86** (2012) 114016, [1207.6066].

[22] **CMS Collaboration** Collaboration, *V Tagging Observables and Correlations*, Tech. Rep. CMS-PAS-JME-14-002, CERN, Geneva, 2014.

[23] P. T. Komiske, E. M. Metodiev, and M. D. Schwartz, *Deep learning in color: towards automated quark/gluon jet discrimination*, *JHEP* **01** (2017) 110, [1612.01551].

[24] J. Cogan, M. Kagan, E. Strauss, and A. Schwartzman, *Jet-Images: Computer Vision Inspired Techniques for Jet Tagging*, *JHEP* **02** (2015) 118, [1407.5675].

[25] L. de Oliveira, M. Kagan, L. Mackey, B. Nachman, and A. Schwartzman, *Jet-images — deep learning edition*, *JHEP* **07** (2016) 069, [1511.05190].

[26] L. G. Almeida, M. Backović, M. Cliche, S. J. Lee, and M. Perelstein, *Playing Tag with ANN: Boosted Top Identification with Pattern Recognition*, *JHEP* **07** (2015) 086, [1501.05968].

[27] P. Baldi, K. Bauer, C. Eng, P. Sadowski, and D. Whiteson, *Jet Substructure Classification in High-Energy Physics with Deep Neural Networks*, *Phys. Rev.* **D93** (2016), no. 9 094034, [1603.09349].

[28] D. Guest, J. Collado, P. Baldi, S.-C. Hsu, G. Urban, and D. Whiteson, *Jet Flavor Classification in High-Energy Physics with Deep Neural Networks*, *Phys. Rev.* **D94** (2016), no. 11 112002, [1607.08633].

[29] M. Bahr et al., *Herwig++ Physics and Manual*, *Eur. Phys. J.* **C58** (2008) 639–707, [0803.0883].

[30] M. Cacciari, G. P. Salam, and G. Soyez, *FastJet User Manual*, *Eur. Phys. J.* **C72** (2012) 1896, [1111.6097].

[31] A. J. Larkoski, J. Thaler, and W. J. Waalewijn, *Gaining (Mutual) Information about Quark/Gluon Discrimination*, *JHEP* **11** (2014) 129, [1408.3122].

[32] P. Bolzoni, B. A. Kniehl, and A. V. Kotikov, *Average gluon and quark jet multiplicities at higher orders*, *Nucl. Phys.* **B875** (2013) 18–44, [1305.6017].

[33] P. Bolzoni, B. A. Kniehl, and A. V. Kotikov, *Gluon and quark jet multiplicities at N^3LO+NNLL*, *Phys. Rev. Lett.* **109** (2012) 242002, [1209.5914].

[34] Y. L. Dokshitzer, F. Fabbri, V. A. Khoze, and W. Ochs, *Multiplicity difference between heavy and light quark jets revisited*, *Eur. Phys. J.* **C45** (2006) 387–400, [hep-ph/0508074].

[35] **ATLAS** Collaboration, G. Aad et al., *The ATLAS Experiment at the CERN Large Hadron Collider*, *JINST* **3** (2008) S08003.

[36] **CMS** Collaboration, S. Chatrchyan et al., *The CMS experiment at the CERN LHC*, *JINST* **3** (2008) S08004.

[37] B. Webber, *Average Multiplicities in Jets*, *Phys. Lett.* **143B** (1984) 501–504.

[38] R. Perez-Ramos and D. d'Enterria, *Energy evolution of the moments of the hadron distribution in QCD jets including NNLL resummation and NLO running-coupling corrections*, *JHEP* **08** (2014) 068, [1310.8534].

[39] D. d'Enterria and R. Pérez-Ramos, *α_s determination at NNLO*+NNLL accuracy from the energy evolution of jet fragmentation functions at low z*, in *Proceedings, 50th Rencontres de Moriond, QCD and high energy interactions: La Thuile, Italy, March 21-28, 2015*, p. 117, 2015. 1505.02624.

[40] B. Bhattacherjee, S. Mukhopadhyay, M. M. Nojiri, Y. Sakaki, and B. R. Webber, *Associated jet and subjet rates in light-quark and gluon jet discrimination*, *JHEP* **04** (2015) 131, [1501.04794].

[41] **OPAL** Collaboration, G. Alexander et al., *A Comparison of b and (uds) quark jets to gluon jets*, *Z. Phys.* **C69** (1996) 543–560.

[42] A. J. Larkoski, G. P. Salam, and J. Thaler, *Energy Correlation Functions for Jet Substructure*, *JHEP* **06** (2013) 108, [1305.0007].

[43] **CMS Collaboration** Collaboration, *Particle-Flow Event Reconstruction in CMS and Performance for Jets, Taus, and MET*, Tech. Rep. CMS-PAS-PFT-09-001, CERN, 2009. Geneva, Apr, 2009.

[44] D. Bertolini, P. Harris, M. Low, and N. Tran, *Pileup Per Particle Identification*, *JHEP* **10** (2014) 059, [1407.6013].

[45] D. E. Soper and M. Spannowsky, *Finding physics signals with event deconstruction*, *Phys. Rev.* **D89** (2014), no. 9 094005, [1402.1189].

[46] **CMS** Collaboration, S. Chatrchyan et al., *Modification of jet shapes in PbPb collisions at* $\sqrt{s_{NN}} = 2.76$ *TeV*, *Phys. Lett.* **B730** (2014) 243–263, [1310.0878].

[47] **CMS Collaboration** Collaboration, *Jet Fragmentation Function in pPb Collisions at sqrt(sNN) = 5.02 TeV and pp Collisions at sqrt(s) = 2.76 and 7 TeV*, Tech. Rep. CMS-PAS-HIN-15-004, CERN, Geneva, 2015.

[48] **CMS Collaboration** Collaboration, *Splitting function in pp and PbPb collisions at 5.02 TeV*, Tech. Rep. CMS-PAS-HIN-16-006, CERN, Geneva, 2016.

[49] G. Brooijmans, P. Schichtel, and M. Spannowsky, *Cosmic ray air showers from sphalerons*, *Phys. Lett.* **B761** (2016) 213–218, [1602.00647].

[50] **Pierre Auger** Collaboration, A. Aab et al., *The Pierre Auger Cosmic Ray Observatory*, *Nucl. Instrum. Meth.* **A798** (2015) 172–213, [1502.01323].